Electric Power Systems Research 197 (2021) 107327

Contents lists available at ScienceDirect

Electric Power Systems Research

journal homepage: www.elsevier.com/locate/epsr

Resiliency-driven strategies for power distribution system development

Illia M. Diahovchenko [a,*], Gowtham Kandaperumal [b], Anurag K. Srivastava [b], Zoia I. Maslova [c], Serhii M. Lebedka [a]

[a] Department of Electrical Power Engineering, Sumy State University, Sumy, 40007, Ukraine
[b] School of EECS, Washington State University, Pullman, WA 99164-2752, USA
[c] Department of Computer Science, Sumy State University, Sumy, 40007, Ukraine

ARTICLE INFO

Keywords:
Resiliency
Distribution system planning
Graph theory
Distributed energy resources
Automated switches
Analytic hierarchy process

ABSTRACT

Power system planning engineers aim to create a reliable, and efficient grid to meet load demand, while avoiding costly investments in advanced distribution technologies. Recent extreme weather and cyber events have exposed the vulnerability of the power grid and posed a new requirement for system resiliency, which denotes its ability to keep serving critical loads even with adverse events. Additionally, a push for integrating distributed energy resources provides multiple opportunities and challenges. The resiliency-driven planning strategies for system resources are still in their infancy, and more investigation is needed. This paper presents a systematic method for enabling highly resilient power distribution systems by suggesting strategies to utilize distributed energy resources and automated switches in efficient way. Topology-based and novel feasible-network-based scores are developed for resiliency measure and to guide selection of appropriate strategies given multiple options. Efficiency of the developed algorithm was substantiated on the modified IEEE 123 node system and provides the most resilient feasible network. The proposed algorithm can be employed by power system engineers for resiliency-driven planning and system upgrades.

Abbreviations and symbols

AC_B	Aggregate Betweenness Centrality
AHP	Analytical Hierarchy Process
BCE	Branch Count Effect
CL	Critical Load
C_n	Clustering coefficient
D	Diameter of a graph
d	Geodesic distance of a graph (i.e. the number of edges)
DER	Distributed Energy Resource
DG	Distributed Generation
F_c	Critical fraction of nodes
FN	Feasible Network
FNRI	Feasible Network Resiliency Index
G	Graph of a power network
l_q	Average path-length
n	Node of a graph
NC	Normally Closed (switch)
NO	Normally Opened (switch)
OB	Overlapping Branches
p_c	Percolation threshold
PCWL	Path Combination Without Loop
PDS	Power Distribution System
PF	Penalty Factor
PNF	Possible Network Fraction
PN	Possible Network
PoA	Probability of Availability
PR	Path Redundancy
RoS	Recurrence of Sources
SO	Switching Operations
TRI	Topological Resiliency Index
λ_2	Algebraic connectivity
ρ	Spectral radius
$\chi(p)$	Susceptibility function of the bond occupation probability
μ	Natural connectivity

* Corresponding author.
E-mail address: i.diahovchenko@etech.sumdu.edu.ua (I.M. Diahovchenko).

https://doi.org/10.1016/j.epsr.2021.107327
Received 29 November 2020; Received in revised form 4 April 2021; Accepted 25 April 2021
Available online 11 May 2021

1. Introduction

1.1. Topicality of resiliency-related studies

A successful transition to a reliable and resilient electricity system requires careful consideration of a range of interrelated issues to meet the expectations of consumers, utilities and society [1]. Continuous and uninterrupted power delivery to the customer is the core aspect of maintaining a high power system reliability and resiliency [2]. Electric energy has become an indispensable entity for industrial production, national security, trade, public transport, hospitals' operation, and communications. Concurrently, the frequency and impact of threats that affect the electric distribution grid is growing. Power outages and blackouts can happen due to unfavorable natural phenomena (e.g. storms, earthquakes, floods, hurricanes) or cyber physical issues (e.g. malicious unauthorized control signals, disruptions in control signal communications). Such unfavorable events could be hazardous, costing billions of dollars and/or human lives.

Data from various studies lead to cost estimates from storm-related outages to the USA economy at dozens billion dollars annually. The weather-related power outages, which took place between 2003 and 2012, cost the American economy more than $300 billion [3]. The total cost of U.S. billion-dollar disasters over the last 5 years (2015-2019) exceeds $525 [4], while until October 2020 there have been 16 devastating natural disasters with losses exceeding $1 billion each to affect the country [5]. In 2015, a synchronized and coordinated cyber-attack compromised three Ukrainian regional electric power distribution companies, and the following outages affected nearly 225 thousand customers [6]. It is evident, that natural disasters and cyber-attacks can cause significant damage of power system, with distribution networks being the most vulnerable sections in confronting natural disasters. Nearly 90% of all hurricane related outages occur in distribution grids [7]. Therefore, many researchers try to find efficient ways to increase distribution grids resiliency against natural disasters, using quick restoration methods [8]. However, an extensive research towards resiliency enhancement is still needed [9, 10].

1.2. Methods to quantify the resiliency

To improve the existing resiliency of the system, the means to quantify it must be determined. Several quantifiable and graph-based metrics for network architectures resiliency estimation are proposed in scientific literature [11]–[14]. The choice of appropriate metrics for the conducted study was made basing on the multiple interacting criteria which affect the resiliency of a power distribution system. Such criteria are available paths and their edge counts, number of available power sources, reconfiguration options, and probability of availability of power sources.

The paper [15] illustrates a time dependent quantifiable resiliency metric in the context of systems and networks. A methodology to assess engineering resiliency and interdependency for subsystems of a multi-system networked infrastructure under extreme natural hazardous events is proposed in [16], and the power outage restoration steps during hurricane Katrina are outlined as an example. In [17] authors developed a framework for resiliency-oriented design for distribution power grids to protect them against devastating natural events, such as earthquakes and inundations. A method to quantify the resiliency of a power distribution system (PDS) using percolation theory and complex network analysis is presented in [18]. Researchers estimated resiliency as an aggregation of four factors [18]: topological resiliency, failure rate of network's equipment, power flow feasibility and intensity of a threat ('weather factor'). In [19] measurement indices to quantify the resiliency of cyber-physical transmission systems are defined. The quantitative model and metrics of distribution electrical grids' resiliency is developed and discussed in [12], where the author considers an analogous measure of availability as a basic metric for resiliency and defines brittleness and resistance as the two key resiliency-related principles. A novel formulation for measuring and enabling resiliency of a PDS is proposed in the article the [13] and examined, using a model of two geographically proximal industry standard CERTS microgrids. And in [20] islanding and fault reconfiguration strategies are applied for resilience enhancement of active distribution networks.

1.3. Planning strategies to enable resiliency of the power distribution system

Several definitions are used in the scientific literature to describe varied conceptualizations of resiliency as well as their limitations. In this paper, the resiliency of the power distribution system is defined as the ability of the network to resist discontinuity of power supply to critical loads (CLs) during stressful operating conditions, and recover from any damages during unfavorable events [21]. CLs are considered as loads that are extremely important for the community, such as hospitals, data centers, fire department, police station, etc. There are multiple ways to increase the resiliency of the power distribution system [9]. For this study planning for injection of distributed energy resources (DERs) (i.e. decentralized energy generation and storage systems placed at or near the point of use) and additional automated switches are chosen.

DERs greatly increase the reliability of the system by helping avoid the impact of a blackout on it. As the penetration of distributed generation (DG) in centralized electricity systems increases, it is in the best interest of utilities to allocate DG in an optimal way so that it improves voltage profile, reforms reliability and reduces losses [22, 23]. To more fully integrate DGs policymakers and utilities should determine prospects to standardize and rationalize interconnection procedures, introduce and implement interoperability standards, and identify the modernization investments preferences to maintain and improve the reliability and flexibility of electrical networks [24, 25]. Distribution system expansion planning strategies encompassing DERs were studied in several scientific papers. The authors had proposed different approaches to find an optimal allocation of DERs, focusing on minimization of the system's power and energy losses [26, 27, 28], dealing with schedulable and intermittent power generation patterns [29], aiming to reduce DG's investment and costs for network upgrading and maintenance [30]. Optimum allocation of different DG technologies and clustering a PDS into a set of microgrids is presented in [31] as a strategy for enhancing reliability and supply-security.

Another way to enhance resiliency is a suitable placement of additional automated tie-line switches, which can increase the number of possible restoration paths in case of a disturbance. Switches can quickly isolate faulted area/areas of a distribution system and redirect power flow to loads. The optimal switch placement problem is a combinatorial problem and involves a nonlinear and non-differential objective function [32]. The methodology for the optimal switch allocation to decrease energy losses and improve service restoration in radial distribution networks is presented in [33, 34]. The allocation of switches to improve reliability is analyzed in [35]. In [36] the placement of remote-controlled switches is considered as a weighed set cover problem, and the method to determine the set of switches to be upgraded for an existing distribution system is proposed. However, in the named papers the positioning of switching devises is was focused on power system's reliability satisfaction. This work presents a systematic approach for PDS planning with respect to resiliency performance and gives an insight on DERs integration and additional automated switches installation from the resiliency perspective.

The proposed methodology for resiliency-driven grid planning is aimed to assure uninterrupted supplyy тwфы reinforcement by means of additional switch placement and deployment of distributed energy resources. In order to quantify the feasibility of a planning decision, a resiliency score is used. The resiliency factors are estimated using graph theoretic means and distribution system analysis, and weighted according to their impact on the power system. The scores are computed

with the multi-criteria decision-making tool, analytical hierarchy process (AHP). The main contributions of the approach proposed in this study can be summarized as follows:

- Developing a comprehensive method for enabling high-resilient power distribution networks.
- Assessing the impact of additional DERs and tie-lines with automated switches on the resiliency performance of power distribution networks.
- Proposing an algorithm, which employs composite topology-based and feasible-network-based resiliency indices, to quantify the feasibility of a planning decision in terms of resiliency performance of a power system.

The rest of the paper is organized as follows. The applied methodology and the proposed algorithm are defined in Section 2. Descriptions of the test model and simulation tools are given in Section 3. The simulation procedure and results are discussed in Section 4. The efficiency of the proposed method is examined with contingency scenarios and devastating natural events in Section 5 55followed by conclusions in Section 6 and Appendix.

2. Methodology and proposed algorithm

For the purposes of distribution network development and resource planning two resiliency assessment approaches were chosen: 1) topology-based, and 2) feasible network (FN)-based [37]. The first approach is based on topological resiliency calculation using graph theory postulates and is inspired by the methodology from [18]. In this study the fusion of topology-based indicators (i.e. metrics) is applied to come up with an independent comprehensive indicator – topological resiliency index (TRI). In contrast to [18], the 'weather factor' is not considered in the TRI equation due to its limited representativeness, given that each 'low-frequency & high impact' threat has a unique nature, and it is difficult to generalize unfavorable events into a certain coefficient [38]. Additionally, relative importance of key factors to determine composite resiliency index was estimated using the semantic Saaty scale [39], which allows to avoid additional computations of dominant eigenvector and liner transformation needed to obtain crisp scores or make transitions to fuzzy scores based on fuzzy judgements, as in [18].

Basing on the hypotheses and resiliency estimation approaches, introduced in [37], FN-based resiliency metrics were mathematically formulated. These metrics are presented in Section 2.2 and can be employed as a mathematics-based structured technique for organizing and analyzing complex decisions. The FN is defined as an operationally feasible configuration of the studied PDS, which can be formed with a certain combination of switches, is able to serve all the CLs, and satisfies the radiality criteria and the operation constraints. FNs can be derived from possible networks (PNs), which have the traits of the FN except of the constraints satisfaction. Thus, the PN is a broader term: each FN is simultaneously a PN, while a PN cannot be a FN by default. After FN-based indicators for different network planning scenarios are calculated, a composite feasible network resiliency index (FNRI), representing the state of the whole power grid, can be obtained.

For the following analysis, the PDS is considered as a graph $G(N, E)$ with N vertices and E edges. The descriptions of each chosen approach and explanations to the metrics choice are given further.

2.1. Topology-based resiliency metrics

Several indicators of network efficiency (diameter, average path length, natural connectivity), redundancy (clustering coefficient) and robustness (aggregate betweenness centrality, algebraic connectivity, clustering coefficient, critical fraction of nodes) were chosen to build up a comprehensive topological resiliency metric. These indicators capture some key topological characteristics of the PDS (i.e. efficiency, redundancy, robustness) and are informative and versatile for the analysis conducted in this work. Definitions and mathematical expressions for the selected metrics are provided below.

1) The *diameter D* of a graph G is the maximum geodesic distance d (i.e. the number of edges) in the shortest path that connects two most remote nodes [40]. It can be represented as

$$D = \max\left\{d\left(n_i, n_j\right) : \forall\left(n_i, n_j\right) \in N\right\}, \tag{1}$$

where n_i and n_j are nodes of the graph G.

2) Aggregate Betweenness Centrality (AC_B) is defined as the average difference betweenness centrality between the most central vertex n of the graph, which has the highest value of betweenness, and all others [41]. For node n_i it can be calculated by

$$AC_B(n_i) = \frac{\sum_{n=1}^{N} \Omega_{n_i}^{q} \cdot \sum_{i \neq n \neq} \frac{\sigma_{ij}(n_i)}{\sigma_{ij}}}{N}, \tag{2}$$

where σ_{ij} is the total number of shortest paths from node i to node j; $\sigma_{ij}(n_i)$ is the number of those paths through the node n_i; Ω_{ni}^{q} is the degree of node n_i in the q-th network configuration. AC_B metric represents the concentration of the network topology around a central location.

3) Algebraic Connectivity λ_2 is the second smallest eigenvalue of normalized Laplacian matrix (i.e. degree matrix minus adjacency matrix) of the network. It quantifies the network's structural robustness and fault tolerance [42]. Larger values of λ_2 correspond to enhanced fault tolerance and robustness against network partition (division into islands).
4) The critical fraction of nodes Fc is determined as a fraction of nodes, which is expected to be sufficient for critical loads supply after a random amount of nodes has been damaged due to an unfavorable event [18]. This metric is closely related to a percolation threshold. The percolation model assumes the presence of an underlying network structure, where nodes (site percolation) or links (bond percolation) are independently occupied with probability p. Nearest-neighbor occupied sites or bonds build clusters so, that for $p = 0$ only clusters of size one can be found in the system, while for $p = 1$ a unique giant cluster spans the entire network [43].

During normal condition, when all components are working as they should be, p equals 1. During a severe unfavorable event, all the nodes of the distribution system are affected, such that each node is functional with a probability p and damaged with a probability $1 - p$ [18]. At intermediate values ($0 < p < 1$) the network can be found in two different phases: a) the nonpercolating mode, where the number of nodes within each cluster is much smaller than the size of the network; b) the percolating mode, where a single macrocluster, which is commensurate in size with the entire network, is formed. The network-dependent quantity, that separates these two phases, can be referred as a *percolation threshold*. It is commonly used to study network robustness against random failures and is usually denoted by p_c [43]:

$$p_c = \arg\left\{\max_{p} \chi(p)\right\}, \tag{3}$$

where $\chi(p)$ is the susceptibility function of the bond occupation probability p.

Thus, for $p < p_c$ a spanning cluster, proportional to the size of the

entire network, exists, while for $p > p_c$ the PDS is fragmented into small clusters. According to Molloy-Reed criteria, the scenario when at least critical loads are fed during a fault (or multiple faults) in a studied network, can be observed if percolation threshold can occur [44]. Given that, in this paper the critical fraction of nodes is defined as

$$F_c \equiv p_c = 1 - \frac{1}{k_0 - 1}, \tag{4}$$

where k_0 is the ratio $\langle k^2 \rangle / \langle k \rangle$ [14], which must be calculated from the pre-perturbed graph, i.e. before the removal of any sites [45]; $\langle k \rangle = 2\frac{|E|}{|N|}$ is the first moment of the degree distribution of G, which represents the average degree of the nodes in the distribution grid; $\langle k^2 \rangle$ is the second moment of the degree distribution of G, which reflects the variance measuring the spread in the degree and defined as the square of the standard deviation of $\langle k \rangle$. According to [45], percolation threshold transition is observable when $\langle k^2 \rangle$ is 2 times as big as $\langle k \rangle$.

1) Average path-length l_q estimates the shortest distance d (i.e. the minimum number of branches) that need to be traversed in order to reach a node n_j from a node n_i [46]

$$l_q = \frac{1}{N(N-1)} \sum_{i,j} d(n_i, n_j) \tag{5}$$

This metric will provide a limited view of network reachability and efficiency in power distribution systems.

1) The clustering coefficient C_n of a certain topology of the graph G is defined as the average of the local clustering coefficients for all the nodes in G [40]

$$C_n = \frac{1}{N} \sum_{i \in N} \frac{y_i}{\binom{d_i}{2}}, \tag{6}$$

where y_i is the number of links between neighbors of n_i; d_i is the degree of the node n_i. This value represents the probability that two neighbors of a node are neighbors themselves.

1) The spectral radius ρ is the largest absolute value among the eigenvalues of the adjacency matrix of the graph G [47]

$$\rho = \max_{1 \le i \le N} |\lambda_i| \tag{7}$$

The smaller the spectral radius, the higher the robustness of a network, and the better it is protected against cyber-attacks [48].

1) Natural connectivity $\bar{\mu}$, is a scaled average eigenvalue of the graph adjacency matrix [49]

$$\bar{\mu} = \ln \left[\frac{1}{n} \sum_{j=1}^{n} e^{\mu_i} \right], \tag{8}$$

where μ is the i-th eigenvalue of the adjacency matrix.

Larger values of μ μ correspond to higher strength (robustness) to branch or node removals.

It can be noted that the topology-based indicators define interrelations between vertices and edges within a single interconnected graph $G(N, E)$ (i.e. within a single interconnected PDS). Since the network's integrity is crucial for topological metrics, their appropriateness for defining resiliency of PDS with microgrids [18] is arguable, which will be additionally examined through this study. Moreover, the introduced topology-based metrics consider network's anatomy, while ignoring the quantity and the availability of sources. Therefore, these metrics can be suggested for PDS planning strategies aimed on the additional switches' installation, and they are less applicable for DERs deployment.

2.2. FN-based resiliency metrics

Elaboration of primary FN-based indicators was inspired by the previous studies [13, 14, 37]. Mathematical expressions of the developed FN-based metrics are introduced further.

1) *Branch Count Effect* (BCE). This is represented by the ratio of the total number of connected branches for each path combination without loop (PCWL) in a possible network to the number of all critical loads. For each PN, the average value of all corresponding similar PNs is considered.

$$BCE_q = \frac{1}{N_q M_q} \sum_{i=1}^{N_q} \sum_{j=1}^{M_q} \mu_{ij}, \tag{9}$$

where μ_{ij} is the length of the valid path p_{ij}, which connects the source with the critical load (CL) in the i-th possible network P_i, and it is equal to $\mu_{ij} = \sum_{e_z \in p_{ij}} e_z$; e_z is the z-th edge of the valid path p_{ij}; the subscript q represents the q-th feasible network being considered, q=1…Q; Q is the total number of FNs; N_q is the total number of PNs for the q-th FN, M_q is the total number of critical loads in the q-th FN.

2) *Overlapping Branches* (OB) is the total number of common branches in each PCWL in a PN. The average value of all similar PN is considered for the corresponding FN.

$$OB_q = \frac{1}{N_q} \sum_{i=1}^{N_q} \sum_{j=1}^{M_q} E_{ij}, E_{ij} \in \cap_j p_j or E_{ij} \in p_1 \cap p_2 \cap \ldots \cap p_{M_q}, \tag{10}$$

where E_{ij} is the sum of the 'critical' (i.e. overlapping) edges in the i-th PN P_i.

3) *Switching Operations* (SO) is the total number of changes in status of the switches, to create different FNs and feed all CLs.

$$SO_q = \sum_{b=1}^{B} \left| S_b^1 - S_b^q \right|, q = 1 \div Q, \tag{11}$$

where the subscript b represents the order of the switch; B is the number of switches (breakers) in the q-th FN; ${S^1}_b$ is the state of the b-th switch in the first (initial) FN (equals 1 if the switch is closed and 0 if opened); ${S^q}_b$ is the state of the b-th switch in the q-th FN.

4) *Recurrence of Sources* (RoS). It refers to the ratio of the number of available sources used to supply all CLs to the number of all CLs in each PN. The average value of all similar PNs is considered for the corresponding FN.

$$RoS_q = \frac{1}{N_q M_q} \sum_{i=1}^{N_q} \left(\sum_{j=1}^{M_q} A_i + 1 \right), A_i = \begin{cases} 1, v_{i1}^1 \neq v_{ij}^1 \\ 0, v_{i1}^1 = v_{ij}^1 \end{cases} \quad (12)$$

Here A_i represents the verification of equality, $v^1{}_{i1}$ is the first vertex of the valid path p_{i1}, $v^1{}_{ij}$ is the first vertex of the valid path p_{ij}.

5) *Path Redundancy* (PR) is defined as the ratio of total number of paths available for all CLs connecting to all sources to the total number of CLs in each FN.

$$PR_q = \frac{|T_q|}{M_q}, \quad (13)$$

where the $|T_q|$ is the cardinality of available sources in the q-th FN.

6) *Probability of Availability and Penalty Factor (PoA & PF):* This factor has two components to distinguish the source feeding power to the CL. PoA is based on reliability of the source, and the PF is based on the losses in distribution. If the CL is drawing power from the main grid, the PoA & PF should be highest because main grid will be more reliable compared to DGs. However, reliability of all DGs to supply a CL may be assumed same but a high penalty should be considered, if power is drawn from a DG located in other MG than from a DG located in same MG, where CL is located.

$$PoA\&PF_q = \frac{1}{N_q M_q} \sum_{i=1}^{N_q} \sum_{j=1}^{M_q} PoA_{ij} \cdot PF_{ij},$$

$$PoA_{ij} = \begin{cases} 0.98, v_{ij}^1 = 1 \\ 0.95, v_{ij}^1 \neq 1 \end{cases} \quad (14)$$

$$PF_{ij} = \begin{cases} 0.9, v_{ij}^1 = 1 \\ 1, v_{ij}^1 \neq 1, \mu_{ij} \leq \chi, v_{ij}^1 \in \mu_{ij} \\ 0.8, v_{ij}^1 \neq 1, \mu_{ij} > \chi, v_{ij}^1 \in \mu_{ij} \end{cases}$$

where χ is some critical number of edges in the μ_{ij}, which should be intuitively evaluated by a user, basing on network's structure.

7) *Possible Network Fraction* (PNF): This is the number of possible networks with similar switch configurations, which can be combined in a one FN.

$$PNF_q = \frac{N_q}{M_q} \quad (15)$$

8) *Aggregate Betweenness Centrality* (AC_B), as defined by (2). This metric was chosen for both topological-based and FN-based resiliency, since it substantially captures the information about the importance of the nodes in a given network's pattern and can be referred to both sets of indicators.

2.3. Algorithm

For enabling resiliency through feasible network solutions and their resiliency quantification, the modified algorithm from [37] was implemented. Since the network topology should be based on its feasibility, the same algorithm can be applied for topology-based resiliency estimation. In such a case each FN will represent a unique grid topology. The applied algorithm is shown in Fig. 1.

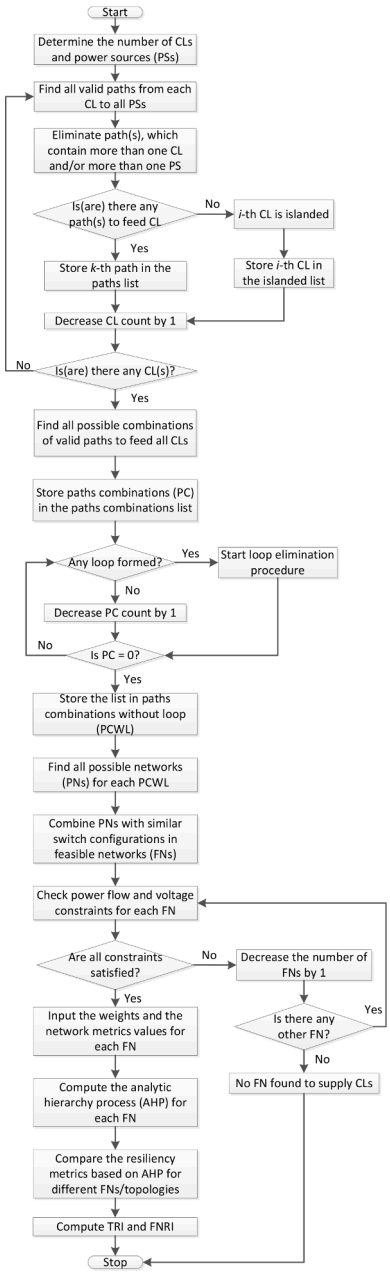

Fig. 1. Algorithm for enabling resiliency through feasible network solutions and their resiliency quantification

To determine the operationally feasible network solutions to serve all critical loads during normal operation and contingencies, at first it is necessary to determine the CLs and available power sources. At the next step all possible paths from critical load to all sources are to be found, and paths containing more than one CL and/or more than one source are to be eliminated. The code written in Python was employed for valid paths search. To maintain the radial nature of the power distribution system, the paths with loops must be removed from the list. For this purpose the loop elimination technique [46] was implemented. On the next stage possible network configurations without loops and with similar switch configurations are combined in sets. Each set corresponds

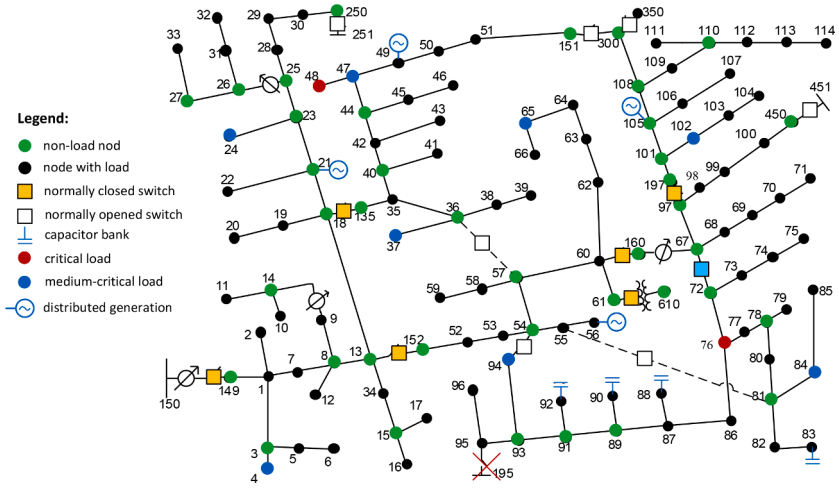

Fig. 2. Modified IEEE 123 node test feeder with 4 DERs and additional switches depicted

to a unique feasible network. Afterwards the power flow calculations and constraints checking are to be made in GridLAB-D and MATLAB Simulink. The Simulink model was created in compliance with [47] and adjusted in accordance with the current study's objectives. The similarity of the calculation results extracted from both GridLAB-D and MATLAB Simulink was considered as a proof of correct simulation. Feasible networks, which satisfy all the operation constraints, are to be stored, and the resiliency quantification is to be performed for each FN. Such a resiliency quantification should be based on the earlier introduced topology-based or FN-based resiliency metrics. An insight about the resiliency performance of the PDS can be obtained from corresponding composite resiliency indexes (i.e. TRI and FNRI), which can be determined in the following several steps.

Topological resiliency of a power distribution network depends on the eight graph-theory-based metrics introduced in Section 2.1. All the metrics are interdependent, and they change with the transformation of the network's configuration. The vector $\overrightarrow{\Re}_T$ provides insights into the topological resiliency of each given FN.

$$\overrightarrow{\Re}_T = \left[D, AC_B, \lambda_2, F_c, l_q, C_n, \rho, \overline{\mu}\right] \tag{16}$$

Obviously, not all metrics capture aspects of resiliency equally good. Since unique numerical solutions are preferred for easier interpretation, the Analytic Hierarchy Process is a feasible approach to quantify resiliency based on the defined criteria. The process of resiliency estimation using AHP implies assigning weights to the network metrics. Then the method organizes the criteria in a hierarchical manner to satisfy the multi-criteria analysis [14]. The criteria were compared pairwise, using the semantic Saaty scale [39], which indicates how many times more important one criteria over another with respect to the primary goal of resiliency assurance. The dominance of one particular metric over others is to be defined by a user (e.g. distribution system operator), basing on his/her experience and awareness on the system's state. The pairwise comparison was then checked for consistency to ensure the user-defined comparisons provide proper results. An inconsistency of 10% is tolerated in AHP. In the next step the output resiliency values $\Re_T$ for each topology are to be obtained. For n feasible architectures a composite topological resiliency index of the whole power grid can be calculated as

$$TRI = \Re_T^{\max} + \left(1 - \Re_T^{\max}\right) \sum_{q=1}^{n-1} w_q \Re_{Tq}, \tag{17}$$

where $\Re_T^{\max}$corresponds to the network configuration with the highest topological resiliency value; $\Re_{Tq}$ is the topological resiliency value of the q-th FN, which is lower than the maximum one; w_q is the normalized weight assigned to the q-th resilient configuration $\Re_{Tq}$. Values of w_q must be assigned to resilient configurations in a descending order and, obviously, their sum must be less than 1 in order to obtain a non-distorted TRI, which obeys the inequality $0 \leq \text{TRI} \leq 1$. In this paper the normalized weights were calculated on the basis of a geometric progression so that

$$w_q = w_1 (1/2)^{q-1}, \tag{18}$$

where $w_1 = 1$ is the normalized weight of $\Re_T^{\max}$.

FN-based resiliency of a power distribution network depends on the eight metrics discussed in Section 2.2. The vector $\overrightarrow{\Re}_{FN}$ provides insights into the feasible-network-based resiliency of each given FN:

$$\overrightarrow{\Re}_{FN} = [BCE, OB, SO, RoS, PR, PoA\&PF, PNF, AC_B] \tag{19}$$

Similarly, AHP was chosen to make the resiliency evaluation of a certain FN, and pairwise comparison coefficients have been assigned to each element of $\overrightarrow{\Re}_{FN}$.

For n FNs a composite resiliency index of the whole power grid can be calculated by the equation

$$FNRI = \Re_{FN}^{\max} + \left(1 - \Re_{FN}^{\max}\right) \sum_{q=1}^{n-1} w_q \Re_{FNq}, \tag{20}$$

where $\Re_{FN}^{\max}$ corresponds to the network configuration with the highest FN-based resiliency value; $\Re_{FNq}$ is the FN-based resiliency value of the q-th FN, which is lower than the maximum one; w_q is the normalized weight assigned to each q-th resilient configuration $\Re_{FNq}$ in a descending order. The sum of w_q must be less than 1 in order to obtain a result, which obeys the inequality $0 \leq \text{FBRI} \leq 1$.

2.4. Operation constraints

Each network configuration should satisfy operation constraints, e.g., power balance, voltage limit at each node, feeder current capacity limits. It can be noted that constant load demand values are considered in this work. To model a different operating state of the PDS, power flow should be recalculated for a different snapshot of load demand values.

Voltage limits constraints

$$\left|V_i^{\min}\right| \leq |V_i| \leq \left|V_i^{\max}\right| \tag{21}$$

Branch capacity constraints

$$\begin{aligned} |I_{fi}| &\leq \left|I_{fi}^{\max}\right| \\ |I_{ri}| &\leq \left|I_{ri}^{\max}\right| \end{aligned} \tag{22}$$

Table 1
Distribution network development scenarios description.

Case name	Description
Base case	The modified IEEE 123 bus system topology with 12 switches and one main source (swing bus 150).
Case 1	Two DERs of 450 kW rated power were injected in the nodes 49 and 56.
Case 2	Three DERs of 300 kW rated power were injected in the nodes 49, 56, and 21.
Case 3	Four DERs of 225 kW rated power were injected in the nodes 49, 56, 21, and 105.
Case 4	Base case, but with two additional normally opened (NO) tie-line switches installed between nodes 36 and 57 and between nodes 55 and 81.
Case 5	Combination of Case 4 and Case 1.
Case 6	Combination of Case 4 and Case 2.
Case 7	Combination of Case 4 and Case 3.

DG real and reactive power constraints

$$P_{DG}^{\min} \le P_{DG} \le P_{DG}^{\max}$$
$$Q_{DG}^{\min} \le Q_{DG} \le Q_{DG}^{\max} \quad (23)$$

In the equations (21)-(23) V_i is the voltage in the i-th node, I_{fi} is the forward flow capacity of the i-th distribution line; I_{ri} is the reverse flow capacity of the i-th distribution line; P_{DG} and Q_{DG} are the available real and reactive power capacities of the injected DGs. Indices *min* and *max* represent the maximum and minimum allowable limits of the corresponding values. It is accepted in this work that voltage deviations should not exceed ±0.05 p.u. violation threshold [50].

3. Case study description

The proposed algorithm for resiliency computation has been tested on the modified IEEE 123 node test feeder, which represents the unbalanced and multi-phase radial distribution network with 11 (originally) three-phase switches and load demand values as per [51] and is shown in Fig. 2. To increase the number of possible paths from the sources to CLs and to avoid loops formation, an additional normally closed (NC) switch was placed between the nodes 67 and 72. In Fig. 2 this switch is displayed as a blue-colored one.

Seven different scenarios (cases) of the distribution network development were formulated, and descriptions of the considered cases are given in Table 1. Cases are designed on the basis of expedient ways of network development with respect to the aim of its resiliency increase. These ways imply injection of additional DERs and allocation of redundant automated NO tie-switches across the network. DERs were deployed in the nodes, which are more likely to be present in as many PNs as possible, and positions for new switches were chosen with regard to the optimal switch allocation principles presented in [34]. Also it is assumed, that the distribution capacity into a geographic space is limited, and therefore some areas are excluded from the consideration for DG deployment. DERs deployment scenarios start with Case 1 by injection of two DG units. Here the quantity of two corresponds to the principle that an independent DER is required to feed each CL, which was described earlier in Section 2.3 and reflected in Fig. 1.

MATLAB Simulink was used for simulations of the studied PDS. The structure of the modified IEEE 123 node test feeder modeled in MATLAB Simulink is shown in Appendix, Fig. A1, and the explanations to elements' reference designations are given in Appendix, Table AI. The weather data is not embedded to the model, and it is assumed that the DERs continuously operate at their rated power ratings, without disruptions or power quality distortions.

4. Simulation results and discussion

According to the algorithm Fig. 1, in the first step all the valid paths must be determined. For this purpose the depth-first search algorithm was applied to the graph of the modified IEEE 123 bus system (Fig. 2). First, consider Cases 1-3, where the system is reinforced by means of additional DG installation. After elimination of loops and paths which contain more than one CL or/and more than one power source, possible networks were obtained: 2 PNs for Base case, 17 PNs for Case 1, 31 PNs for Case 2, and 47 PNs for Case 3. Some of the PNs have the same switch configurations. Thus, they are combined into six unique feasible networks. The list of possible networks and their combinations to feasible networks are shown in Appendix, Table AII.

Table 2
The color map for PNs and performed studies conformance.

	No DERs
	2 DERs & 2 CLs
	3 DERs & 2 CLs
	4 DERs & 2 CLs

The color map Table 2 corresponds to the studied cases. The unique network configurations with corresponding switch configurations for these six FNs are shown in Table 3. The 0 corresponds to a normally opened switch, while the 1 corresponds to a normally closed switch. Numbers of switch operations (SO) are provided as well.

Note that not all colors from Table 2 are present in Table 3 for FN color selection. This can be clarified with an example. FN1 topology can be formed in the Base case and in Cases 1-3, but in Table 3 FN1 is highlighted in purple, which corresponds to the simplest scenario needed to make FN1 viable. The same is true for the FN3: it can be formed in Case 1 and Case 2, but only Case 1 with PN3 and PN15 is necessary for its existence, while Case 2 just adds one more possible network PN26.

Secondly, consider Case 4, where the system is reinforced with additional automated switches. Nine PNs were obtained, which correspond to nine unique FNs. The unique feasible network configurations with all the sectionalizing and tie-line switches statuses are placed in Table 4 (FN1_sw–FN9_sw). Here and further the subscript '_sw' states for presence of the additional switches. The 0 corresponds to a NO switch, while the 1 corresponds to a NC switch.

Next, consider Cases 5-7, where the system is reinforced by means of additional DG and switches combining. After elimination of loops and paths that contain more than one CL or/and more than one power source, possible networks were obtained: 54 PNs for Case 5, 106 PNs for Case 6, and 157 PNs for Case 7. Some PNs have the same switch configurations. Thus, they are combined in thirteen unique feasible networks (see Appendix, Table AIII).

Here purple highlight corresponds to the Case 4, where just additional switches are present. The unique feasible network configurations with all the sectionalizing and tie-line switches status for Cases 5-7 are shown in Table 4. FN1_sw–FN9_sw are the same as for the Case 4, while four unique configurations FN10_sw–FN13_sw can appear only when two DERs are added (Case 5).

All the six unique feasible networks in Table 3 and all the thirteen feasible networks in Table 4 are operationally feasible with ±0.05 p.u. bus voltage violation threshold. Thus, the topological resiliency metrics can now be quantified for all the unique topologies, and then the TRI can be found. As far as none of the topology-based metrics from Section 2.1 takes into account the number of sources and paths between the sources and the CLs, the only topology of the modified IEEE 123 bus system is required as the input. In this paper FNs from Table 3 and Table 4 represent different possible topologies. By comparison of FNs' switch statuses, it can be noted that there are four FNs from Table 3, which are similar to four FNs from Table 4. Besides, to create a FN5 from Table 3 the studied IEEE 123 node distribution network must be split into two microgrids, which operate in an islanded mode or, likewise, one part is interconnected with the swing bus 150, while the other one is isolated.

Table 3
Switches status for Base case and Cases 1-3.

Switch number		13-152	18-135	60-160	61-610	97-197	150-149	67-72	54-94	151-300
FN	SO	Switch status for saving CL1 (48) and CL2 (76)								
FN1	0	1	1	1	1	1	1	1	0	0
FN2	2	1	1	**0**	1	1	1	1	**1**	0
FN3	2	1	1	**0**	1	1	1	1	0	**1**
FN4	4	**0**	1	1	1	1	1	**0**	**1**	**1**
FN5	3	**0**	1	1	1	1	1	**0**	**1**	0
FN6	2	1	1	1	1	1	1	**0**	**1**	0

Table 4
Switches status for Cases 4-7.

Switch number		13-152	18-135	60-160	61-610	97-197	150-149	67-72	54-94	151-300	36-57	55-81
FN	SO	Switch status for saving CL1 (48) and CL2 (76)										
With additional automated switches												
FN1_sw	2	**0**	1	1	1	1	1	1	0	0	**1**	0
FN2_sw	0	1	1	1	1	1	1	1	0	0	0	0
FN3_sw	2	1	1	1	1	1	1	**0**	**1**	0	0	0
FN4_sw	2	1	1	1	1	1	1	**0**	0	0	0	**1**
FN5_sw	4	**0**	1	1	1	1	1	**0**	**1**	0	**1**	0
FN6_sw	4	**0**	1	1	1	1	1	**0**	0	0	**1**	**1**
FN7_sw	2	1	**0**	1	1	1	1	1	0	0	**1**	0
FN8_sw	4	1	**0**	1	1	1	1	**0**	**1**	0	**1**	0
FN9_sw	4	1	**0**	1	1	1	1	**0**	0	0	**1**	**1**
With DERs & additional automated switches												
FN10_sw	2	1	1	**0**	1	1	1	1	0	**1**	0	0
FN11_sw	4	**0**	1	1	1	1	1	**0**	**1**	**1**	0	0
FN12_sw	4	**0**	1	1	1	1	1	**0**	0	**1**	0	**1**
FN13_sw	4	1	**0**	**0**	1	1	1	1	0	**1**	**1**	0

Table 5
Topology-based network metrics.

Topology No	Corresponding FN	D	AC_B	λ_2	F_c	l_q	C_n	ρ	$\overline{\mu}$
Topology 1	FN1, FN2_sw	30	0.4970	0.0031	2.5528	12.6443	1.4046	6.1097	0.8537
Topology 2	FN2	35	0.5301	0.0027	2.5528	13.3809	1.4046	6.1097	0.8537
Topology 3	FN3, FN10_sw	39	0.5940	0.0020	2.5171	15.3346	1.4148	6.1097	0.8522
Topology 4	FN4, FN11_sw	42	0.6528	0.0018	2.5347	16.6250	1.4198	5.7848	0.8528
Topology 5	FN6, FN3_sw	30	0.4934	0.0041	2.5712	12.3998	1.4097	6.1097	0.8544
Topology 6	FN1_sw	25	0.4709	0.0039	2.5902	11.4915	1.3944	6.1427	0.8553
Topology 7	FN4_sw	30	0.4887	0.0041	2.5902	12.3756	1.3944	6.1097	0.8552
Topology 8	FN5_sw	28	0.4805	0.0052	2.6096	11.5934	1.3995	6.2621	0.8561
Topology 9	FN6_sw	28	0.4799	0.0052	2.6294	11.5692	1.3842	6.1538	0.8568
Topology 10	FN7_sw	27	0.4828	0.0038	2.5902	12.0923	1.3944	6.1384	0.8553
Topology 11	FN8_sw	28	0.4840	0.0049	2.6096	11.9594	1.3995	6.2597	0.8561
Topology 12	FN9_sw	28	0.4793	0.0049	2.6294	11.9352	1.3842	6.1498	0.8568
Topology 13	FN12_sw	42	0.6521	0.0018	2.5528	16.6008	1.4046	5.7848	0.8535
Topology 14	FN13_sw	40	0.6413	0.0018	2.5528	16.2539	1.4046	5.9881	0.8537

In this case diameter D and average path length l_q metrics become infinite, and their calculation is possible only separately, i.e. individually for each microgrid/part, which raises a challenge to find a way to compare topology of FN5 with other topologies on a resiliency basis. Thus, the topological metrics cannot be applied for defining resiliency of the FN5 and are appropriate for resiliency estimation of connected

Table 6
The influence of the network metrics on resiliency scores.

Topology-based resiliency metrics								
Influence on TRI	D	AC_B	λ_2	F_c	l_q	C_n	ρ	$\overline{\mu}$
Positive			•	•		•		•
Negative	•	•			•		•	
FN-based resiliency metrics								
Influence on FNRI	BCE_q	OB_q	SO_q	RoS_q	$PoA_q \times PF_q$	PR_q	PNF_q	AC_B
Positive				•	•	•	•	
Negative	•	•	•					•

Table 7
Pairwise comparison matrix with weight coefficients for topology-based metrics.

Criteria	D	AC_B	λ_2	F_c	l_q	C_n	ρ	$\overline{\mu}$	Weights
D	1	1	0.5	0.16	1	0.33	0.25	0.33	**0.0585**
AC_B	1	1	0.75	0.5	1	1	0.75	1	**0.0985**
λ_2	2	1.333	1	0.5	0.5	1	0.75	1	**0.1048**
F_c	6.25	2	2	1	2	1.5	1.5	2	**0.2263**
l_q	1	1	2	0.5	1	1.5	1.25	1	**0.1294**
C_n	3.03	1	1	0.667	0.667	1	0.5	1	**0.1108**
ρ	4	1.333	1.333	0.667	0.8	2	1	0.75	**0.1459**
$\overline{\mu}$	3.03	1	1	0.5	1	1	1.333	1	**0.1259**

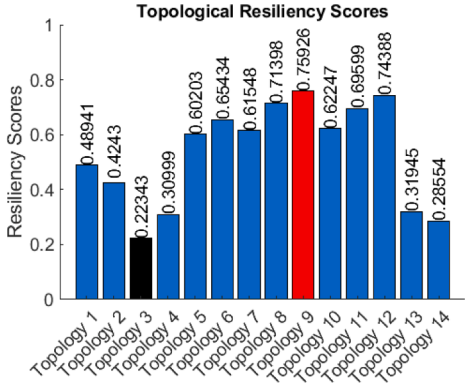

Fig. 3. Topology-based resiliency scores from AHP

distribution networks only. Therefore, the TRI will be used for estimation of resiliency-based switch placement planning. Using this methodology, we can adequately compare the FN1 (Base case) with the feasible networks obtained by additional switches allocation (namely FN2_sw–FN9_sw).

Given that FN5 cannot be considered for topology-based resiliency calculation, it was excluded from the list. Thus, fourteen unique topologies are defined. Results of topology-based metrics computation are listed in Table 5.

While assessing the significance for each criterion, it is essential to take into account that some metrics contribute to strengthen the resiliency, while others decrease it. The influence of the network metrics on topology-based resiliency scores are shown in Table 6. For higher TRI it is necessary to take such system planning or operating actions, that the metrics with negative impact become lower (to be shrunk), while metrics with positive impact become higher (to be risen).

Using the Saaty scale and considering the data from Table 6, the 8 × 8 pairwise comparison matrix (Table 7) was assigned to all the feasible topologies. The inputs are to be subjectively determined by users (e.g. planning engineers, distribution system operators), basing on their experience and awareness about the system's state. All the eight criteria

Table 8
TRI for different network reinforcement scenarios.

Case name	Brief characteristic	TRI scores
Base case	No DG or additional switches	0.5977
Case 1	2 DERs added	0.6516
Case 3	4 DERs added	0.7626
Case 4	Base case + additional switches	0.9312
Case 5	2 DERs + additional switches	0.9314

defined in Section 2.1 are compared pairwise with respect to the objective, which is to maximize the resiliency of the power distribution system.

The AHP scores were obtained using input values and pairwise comparative weights. The degrees of interaction are identified by the significance ratio between maximum and minimum input values of the network metrics. The AHP pairwise comparison matrix has an inconsistency of 3.76%, which satisfies the established 10% inconsistency threshold. The calculated results are shown in Fig. 3.

From Fig. 3 it is seen that Topology 9 demonstrates the highest topology-based resiliency, which corresponds to the FN6_sw from Table 5. The worst performance is assigned to the Topology 3 (FN3, FN10_sw). For different PDS reinforcement scenarios the composite TRI values were calculated by the formula (17). The results are summarized in Table 8. Installation of additional tie-line switches helps to enhance TRI 1.5578 times, compared to the initial stage of the network.

The topology-based resiliency is derived from the graph theory. The TRI and topology-based resiliency indicators are applicable for PDS planning strategies aimed on the additional switches installation, and can provide an insight about how resilient is one particular FN (topology) compared to another. However, for PDS planning strategies focused on DERs deployment the TRI is not applicable since it does not take into consideration the location of sources in regard to CLs. To escape this disadvantage, the topological resiliency vector $\vec{\Re}_T$ can be fortified by some distance-class metrics with assigned nodes or by incorporation of the path length between assigned nodes. Besides, additional studies on topology-based resiliency for PDS development planning can be useful. The existing body of literature has produced some blended upshots

Table 9
Network metrics for FNs for the base case and cases 1-3.

Subcase	Case study	FN	BCE_q	OB_q	SO_q	RoS_q	$PoA_q \times PF_q$	PR_q	PNF_q	AC_B
A1	Base case	FN1	15	6	0	1	0.7779	0.5	0.5	0.7691
A2	Case 1		13	3.8571	0	1.7143	0.7535	3	3.5	0.7691
A3	Case 2		12.4615	3.0769	0	1.8462	0.7467	4	6.5	0.7691
A4	Case 3		12.7143	3.4286	0	1.9048	0.7741	5	10.5	0.7691
A5	Base case	FN2	15.5	4	2	1	0.7779	0.5	0.5	0.6640
A6	Case 1		13.5	3.4286	2	1.8571	0.7535	3	3.5	0.6640
A7	Case 2		12.9615	2.6923	2	1.9231	0.7467	4	6.5	0.6640
A8	Case 1	FN3	13.75	0	2	2	0.6240	3	1	0.6453
A9	Case 2		12.8333	0	2	2	0.6566	4	1.5	0.6453
A10	Case 1	FN4	18	0	4	2	0.6703	3	0.5	0.7822
A11	Case 2		16.75	0	4	2	0.6962	4	1	0.7822
A12	Case 3	FN5	13.125	0.25	3	2	0.8412	5	2	0.6509
A13	Case 3	FN6	18.125	6	2	2	0.7961	5	2	0.7702

Table 10
Pairwise comparison matrix with weight coefficients for FN-based metrics.

Criteria	BCE_q	OB_q	SO_q	RoS_q	$PoA_q \times PF_q$	PR_q	PNF_q	AC_B	Weights
BCE_q	1	1	3	1	0.33	0.2	0.25	0.16	**0.0445**
OB_q	0.33	1	3	1	0.33	0.2	0.25	0.16	**0.041**
SO_q	0.33	0.33	1	1	0.25	0.16	0.2	0.12	**0.0268**
RoS_q	1	1	1	1	0.33	0.2	0.25	0.16	**0.0382**
$PoA_q \times PF_q$	3	3	4	3	1	0.33	0.25	0.16	**0.0856**
PR_q	4	4	6	5	3	1	0.33	0.16	**0.1442**
PNF_q	4	4	5	4	4	3	1	0.25	**0.2008**
AC_B	6	6	8.33	6	6	6	4	1	**0.419**

related to measuring the structure of power networks and connections between topological structure and performance [45, 52, 53]. The analysis of the topological structure of the Western, Eastern, and Texas Interconnects of the North American electric power network, provided in [52], led to the conclusion that power grids are neither scale-free nor small-world in topological structure. Although this inference refers to transmission layer, it casts doubt on the possibility of the tolerance of distribution network to intentional threat analysis, while considering them as scale-free networks with known degree distribution law, as in [45, 53].

On the next stage the FN-based resiliency scores and FNRI are to be obtained. Note that q-th feasible networks from Table 3 and Table 4 will have different resiliency scores for Base case and Cases 1-7, due to changes in the number of available power sources. In case when the CL is being fed from the main grid, Probability of Availability is assumed to be 0.98 and Penalty Factor is assumed to be 0.9, and PoA of each DG is considered 0.95. PF is assumed to be 1, if both DG and CL are close to each other, and PF is assumed to be 0.8, if DG and CL are remote. The closeness estimation is subjective: if a distance between a DER and a CL surpasses 8 nodes, the power source is considered as a remote, otherwise it is close. Due to higher comprehensiveness of this method FN-based resiliency scores were calculated separately for scenarios with DG deployment, additional switch placement, and combination of both actions.

To compare Base case and Cases 1-3 with injection of DG units, 13 subcases A1-A13 were formed. The network metrics are quantified for all the FNs and listed in Table 9. The 8 × 8 pairwise comparison matrix (Table 10) was assigned to all the FNs. The criteria defined in Section 2.2 are compared pairwise with respect to the objective of PDS resiliency maximization. The influence of different indicators on FN-based resiliency scores is shown in Table 7. For higher FNRI indicators with negative impact should be reduced, while indicators with positive impact should be improved.

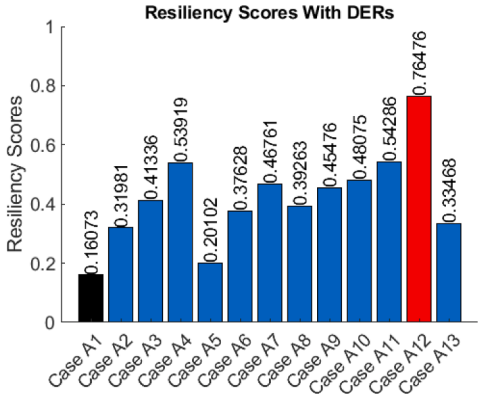

Fig. 4. Resiliency scores for the Base case and Cases 1-3 from AHP

The AHP values were obtained using input values and pairwise comparative weights. The AHP pairwise comparison matrix has an inconsistency of 5.1%, which satisfies the 10% inconsistency threshold, defined earlier. The calculated results are shown in Fig. 4.

The chart clearly shows that FN-based resiliency score moderately increases with DG units added. The FN5 (Case 3 with 4 DERs) has the highest resiliency rate, while FN1 (Base case) has the lowest. The

Table 11
Network metrics for FNs for the case 4 (Base case with additional switches).

Subcase	FN	BCE_q	OB_q	SO_q	RoS_q	$PoA_q \times PF_q$	PR_q	PNF_q	AC_B
B1	FN1_sw	15	7	2	1	0.7779	0.5	0.5	0.7691
B2	FN2_sw	15	6	0	1	0.7779	0.5	0.5	0.6640
B3	FN3_sw	15.5	4	2	1	0.7779	0.5	0.5	0.6453
B4	FN4_sw	15	4	2	1	0.7779	0.5	0.5	0.7822
B5	FN5_sw	16.5	6	4	1	0.7779	0.5	0.5	0.7224
B6	FN6_sw	16	6	4	1	0.7779	0.5	0.5	0.8513
B7	FN7_sw	17	9	2	1	0.7779	0.5	0.5	0.6659
B8	FN8_sw	17.5	7	4	1	0.7779	0.5	0.5	0.6509
B9	FN9_sw	17	7	4	1	0.7779	0.5	0.5	0.7702

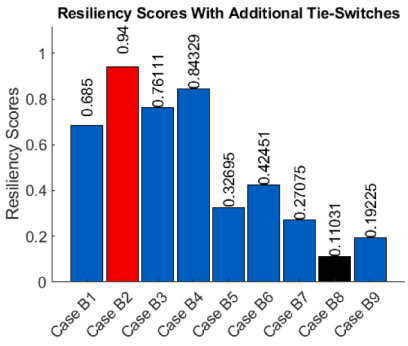

Fig. 5. Resiliency values for PDS with additional tie-switches from AHP

resiliency increase ratio between subcases indexed A12 and A1 is 4.758. Obviously, additional distributed energy sources help to increase systems' reliability and resiliency. However, the criticality of DERs presence and their quantity depends on the network's configuration. To assist power system planners with adding certain amount of DERs, a cost-benefit evaluation of resiliency improvements of the PDS can be used. The cost-benefit analysis can help to compare proposed resiliency-oriented measures and assist in decision-making on whether or not to invest in additional distributed generators, but this aspect is out of the scope of this paper.

Additional tie-line switches provide nine feasible networks, namely FN1_sw–FN9_sw, instead of only two FNs for the Base case, which means more paths are available to supply CLs. The FN-based resiliency metrics are quantified for all the PDS possible configurations for the Case 4. The results are listed in Table 11. The resiliency scores, calculated with AHP, are shown in Fig. 5.

From Fig. 5 it can be summed up, that the most resilient are FN2_sw and FN4_sw, while the worst scenario is FN8_sw. None of the added automated switches are engaged in FN2_sw formation, while for FN4_sw architecture only the connection link between the nodes 55 and 81 is crucial. Thus, to exhibit the influence of additional FNs creation, the FNRI should be calculated, which will be done in the subsequent step.

Finally, the FN-based resiliency scores of the hybrid network reinforcement scenario are to be computed. To compare Cases 4-7 with DG deployment and redundant tie-line switches, 44 subcases C1–C44 were formed. The network metrics are quantified for all the FNs and listed in Table 12. The resiliency scores from AHP are presented as a chart in Fig. 6.

From Fig. 6 it is seen, that subcase C42 demonstrates the highest FN-based resiliency, and the lowest resiliency is supervised in C21, which correspond to the FN12_sw and FN6_sw from Table 12, respectively. Now let us calculate the FNRI by means of the formula (20) for all the considered network reinforcement planning scenarios. Since the charts in Fig. 4, Fig. 5, and Fig. 6 have different scales, the resiliency scores for these cases were transformed to a single scale to make the comparison. After such a unification the maximums of the compared charts are of the same value. The FNRI outputs are summarized in Table 13.

The studied IEEE 123 node PDS has the resiliency rate of 0.2652 for the Base case. The column 'Improvement ratio' indicates the ratio of the FNRI increase with respect to the Base case. For example, injection of DERs in the nodes 49 and 56 helps to enhance the composite resiliency score of the whole network 2.4938 times. Initial PDS replenishment with automated switches rises FNRI 1.4955 times, which complies with the improvement rate, obtained using TRI, with a 4% tolerance. The combined reinforcement by means of 3 DERs and additional switches deployment amplifies the network's resiliency rate 3.4891 times (FNRI = 0.9254), while the fourth DER seems to be excessive, since it does not make a sufficient contribution to FNRI improvement. Preliminary estimation of further PDS reinforcement by means of the DGs number increase to 5 and then to 6 demonstrated scanty FNRI enhancement and, therefore, is inexpedient.

The FNRI is an illustrative instrument, which provides distribution planning engineers with an insight about the resiliency of a PDS and can help to make a pairwise decision about the infrastructural investments. It is directly targeted on CLs saving and takes into account the number and locations of available sources. For the considered modified IEEE 123 bus system, the optimum planning decision lies between Case 3 and Case 6 (see Table 13). Case 6 provides 0.81% better composite resiliency rate, compared to Case 3. However, if the 4 DERs installation cost shows better trade-off than the deployment of 3 DERs and two tie-line switches, than Case 3 also can be considered as a PDS development scenario. As noted earlier, cost-benefit analysis of resiliency-oriented measures is beyond the scope of this work. The following notes summarize the planning and operational strategies to be taken by the distribution system operator (DSO) and network planners for each of the system upgrade scenarios evaluated in Section 4.

- For the initial state of the PDS (i.e. not reinforced) it is suggested to choose the Topology 9 (see Fig. 3) with the switches' statuses as in Table 4.
- For PDS planning strategies aimed on DERs deployment, the Case A12, which corresponds to the FN5 with 4 DERs as per Table 3 and Table 9, has the highest priority (see Fig. 4). The FNRI estimation shows that installation of the 4 complementary generation units allows to enhance resiliency 3.3463 times, compared to the Base case (see Table 13).
- For PDS planning strategies focused on adding tie-lines with

Table 12
Network metrics for FNs for the base case and cases 4-7.

Subcase	Case study	FN	BCE_q	OB_q	SO_q	RoS_q	$PoA_q \times PF_q$	PR_q	PNF_q	AC_B
C1	Case 4	FN1_sw	15	7	2	1	0.7779	0.5	0.5	0.4709
C2	Case 5		13.3	4.4	2	1.8	0.7357	3	2.5	0.4709
C3	Case 6		13.05	3.6	2	1.9	0.7389	4	5	0.4709
C4	Case 7		13.6333	3.6	2	1.9333	0.7202	5	7.5	0.4709
C5	Case 4	FN2_sw	15.5	6	0	1	0.7779	0.5	0.5	0.4970
C6	Case 5		13.4286	3.8571	0	1.8571	0.7535	3	3.5	0.4970
C7	Case 6		13.6923	3.0769	0	1.9231	0.7467	4	6.5	0.4970
C8	Case 7		14.5	3.4286	0	1.9524	0.7438	5	10.5	0.4970
C9	Case 4	FN3_sw	15	4	2	1	0.7779	0.5	0.5	0.4934
C10	Case 5		13.5	3.4286	2	1.8571	0.7535	3	3.5	0.4934
C11	Case 6		13.6923	2.6923	2	1.9231	0.7467	4	6.5	0.4934
C12	Case 7		14.5238	2.8571	2	1.9524	0.7438	5	10.5	0.4934
C13	Case 4	FN4_sw	16.5	4	2	1	0.7779	0.5	0.5	0.4887
C14	Case 5		14.7857	4	2	1.8571	0.7357	3	3.5	0.4887
C15	Case 6		14.4615	3.1538	2	1.9231	0.7331	4	6.5	0.4887
C16	Case 7		14.9762	3.2381	2	1.9524	0.7323	5	10.5	0.4887
C17	Case 4	FN5_sw	16	6	4	1	0.7779	0.5	0.5	0.4805
C18	Case 5		14.1	4.6	4	1.8	0.7068	3	2.5	0.4805
C19	Case 6		14.65	3.8	4	1.9	0.7064	4	5	0.4805
C20	Case 7		14.9	3.5333	4	1.9333	0.6889	5	7.5	0.4805
C21	Case 4	FN6_sw	17	6	4	1	0.7779	0.5	0.5	0.4799
C22	Case 5		14.6	5	4	1.8	0.7068	3	2.5	0.4799
C23	Case 6		14.9	4.1	4	1.9	0.7064	4	5	0.4799
C24	Case 7		15.0333	3.8667	4	1.9333	0.7064	5	7.5	0.4799
C25	Case 4	FN7_sw	17.5	9	2	1	0.7779	0.5	0.5	0.4828
C26	Case 5		15.375	5	2	1.75	0.7391	3	2	0.4828
C27	Case 6		14.8889	4.3333	2	1.8889	0.7408	4	4.5	0.4828
C28	Case 7		15.1923	3.3077	2	1.9231	0.7427	5	6.5	0.4828
C29	Case 4	FN8_sw	17	7	4	1	0.7779	0.5	0.5	0.4840
C30	Case 5		15.625	4.25	4	1.75	0.6972	3	2	0.4840
C31	Case 6		15.6667	3.6667	4	1.8889	0.7021	4	4.5	0.4840
C32	Case 7		15.7692	2.8462	4	1.9231	0.7159	5	6.5	0.4840
C33	Case 4	FN9_sw	13.5	7	4	1	0.7779	0.5	0.5	0.4793
C34	Case 5		13.125	4.75	4	1.75	0.7391	3	2	0.4793
C35	Case 6		14.7222	4.1111	4	1.8889	0.7408	4	4.5	0.4793
C36	Case 7		15.0769	3.1538	4	1.9231	0.7427	5	6.5	0.4793
C37	Case 5	FN10_sw	15.25	0	2	2	0.6240	3	1	0.5940
C38	Case 6		13.8333	0	2	2	0.6566	4	1.5	0.5940
C39	Case 5	FN11 sw	17.5	0	4	2	0.6703	3	0.5	0.6528
C40	Case 6		15	0	4	2	0.6962	4	1	0.6528
C41	Case 5	FN12_sw	11.5	0	4	2	0.6703	3	0.5	0.6521
C42	Case 6		12	0	4	2	0.6962	4	1	0.6521
C43	Case 5	FN13_sw	15.5	0	4	2	0.6240	3	1	0.6413
C44	Case 6		15	0	4	2	0.6566	4	1.5	0.6413

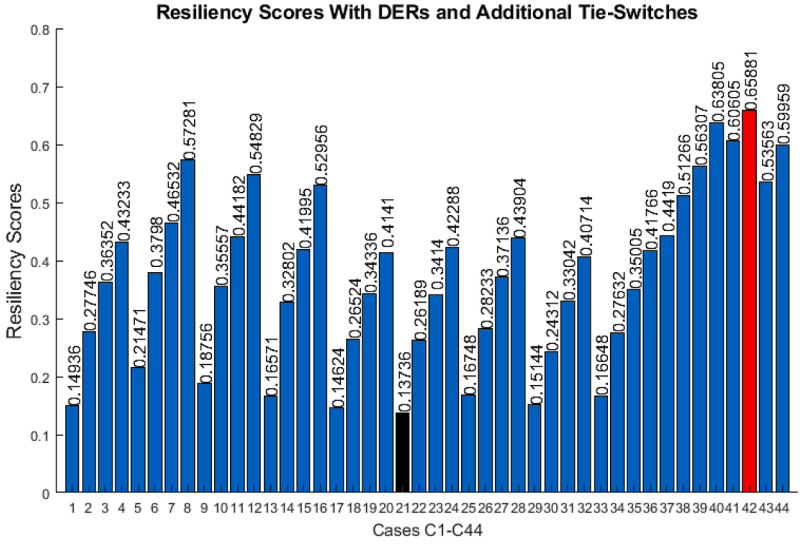

Fig. 6. Resiliency scores for the Cases 4-7 from AHP

Table 13
FNRI for different network reinforcement scenarios.

Case name	Brief characteristic	FNRI scores	Improvement ratio
Base case	No DG or additional switches	0.2652	1
Case 1	2 DERs added	0.6614	2.4938
Case 2	3 DERs added	0.7519	2.8351
Case 3	4 DERs added	0.8875	3.3463
Case 4	Base case + additional switches	0.4022	1.4955
Case 5	2 DERs + additional switches	0.8808	3.3208
Case 6	3 DERs + additional switches	0.9254	3.4891
Case 7	4 DERs + additional switches	0.9329	3.5172

Table 14
Agreement and complementarity of the topology-based and FN-based composite resiliency indicators.

TRI	FNRI
• founded on existing measures in graph theory;	• uses alternative measures, based on the graph theory;
• individual indicators are focused on resiliency performance of the whole system;	• individual indicators are focused on uninterrupted supply of CLs;
• considers the aspects of network's efficiency, redundancy, robustness;	• considers the aspects of remoteness of a CL from sources, reliability, importance of the particular nodes, robustness;
• sensitive to interrelations between nodes and branches and applicable for interconnected PDSs (connected graphs);	• applicable for interconnected feeders and for PDS with microgrids;
• useful for resiliency-driven methods focused on additional tie-lines and/or switches placement, but less applicable for methods focused of DERs deployment	• useful for resiliency-driven methods focused on DERs deployment, as well as for methods focused on additional tie-lines and/or switches placement

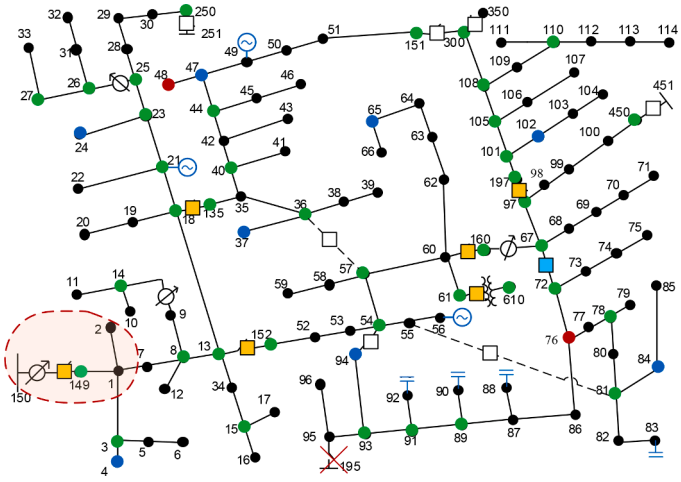

Fig. 7. Contingency I scenario: substation bus 150 and nodes 1, 2 are damaged due to inundation

automated switches, the Case B2, which corresponds to the FN2_sw as per Table 4 and Table 11, ensures the highest resiliency performance (see Fig. 5). Compared to the initial state of the PDS, the TRI improvement ratio is 1.5578, and the FNRI improvement ratio is 1.4955. The TRI and the FNRI scores coordinate with a 4% tolerance.

• The best results can be reached with the hybrid network reinforcement scenario, where both DERs and tie-line switches are injected.

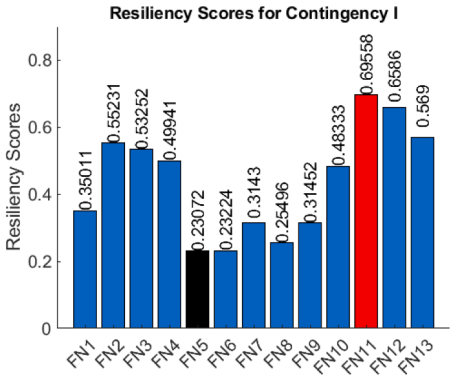

Fig. 8. Resiliency scores for Contingency I scenario

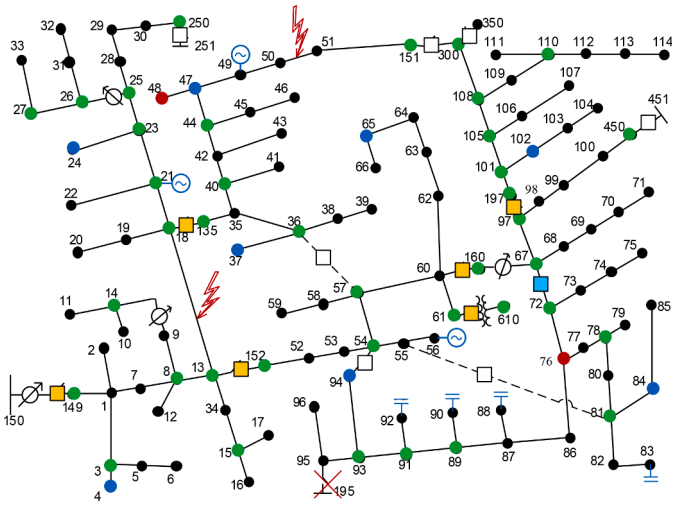

Fig. 9. Contingency II scenario: two faults occur on main, on the lines 13-18 and 50-51

The DSO should adhere to the Case 42 (see Fig. 6), which corresponds to the FN12_sw, as per Table 4 and Table 12. Compared to the Base case, the highest FNRI improvement ratio achieved is 3.5172.

In such a way, the proposed methodology can identify the most resilient feasible network, which should be understood as a configuration with a highest resiliency score (i.e. the highest value of FNRI or TRI) for a particular planning scenario. Basing on the results of the calculations presented in this work, a summary of the applicability and validity the of topology-based vs. FN-based resiliency metrics is provided in Table 14.

5. Contingency scenarios

Using the comprehensive indicators of complex network's resiliency presented in the previous sections, power system engineers will be able to make long-term strategic planning decisions before any contingency occurs. This section is aimed to examine the applicability of the developed algorithm for resiliency-driven operational decision-making (i.e. for post-contingency planning). The resiliency scores presented in this section reflect the ability of the PDS to supply the loads during particular contingency scenarios. In contrast with the applications of the resiliency metrics in Section 4, the following paragraphs describe the resiliency of the power distribution system with respect to possible failures (that

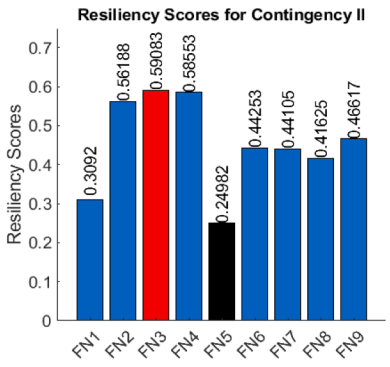

Fig. 10. Resiliency scores for Contingency II scenario

might occur but have not yet).

Given that the PDS subjected to a hazardous event can be split into several parts, the FNRI would be more illustrative for post-contingency operation. In order to demonstrate the usability of the discussed FN-based resiliency metrics to minimize the chances of interruption of CLs supply (i.e. to mitigate the consequences), three different contingency scenarios have been formulated for the modified IEEE 123 node test feeder. For resiliency analysis against contingencies the distribution network FN12_sw, developed according to Case 6 (3 DERs and additional tie-line switches are installed, FNRI = 0.9254), is considered. For the further considered scenarios it is assumed, that when a fault or a hazardous event occurs, the protection system isolates the faulted/damaged area. Note that since the graph of the studied PDS changes after a contingency happens, different FNs can be optimal for different contingencies.

Contingency I: It is assumed that the supply substation bus 150 and nodes 1, 2 are damaged due to a natural unfavorable event, such as an inundation (Fig. 7). The influenced area is circled in a red dotted line. In this case the bulk of the PDS operates as a microgrid in an islanded mode, and nodes 3-6 are unsupplied due to the lost connection. All the thirteen feasible networks listed in Table 12 are operationally possible. However, the number of PNs within these FNs is reduced, and some FN-based resiliency metrics will change. The new resiliency scores for the modified IEEE 123 node test feeder exhibited to this contingency are shown in Fig. 8. Based on that, the distribution system operator should choose the FN11_sw, which corresponds to the highest resiliency mode. To reconfigure the PDS accordingly, the DSO should perform 2 switching operations: to close the switch between nodes 54 and 94 and to open the switch between nodes 55 and 81.

Contingency II: Let us consider the scenario when the three-phase lines 13-18 and 50-51 are tripped due to a fault, e.g. a short circuit (Fig. 9). In this case nine configurations FN1_sw–FN9_sw are feasible. Due to the absence of the line 13-18, there is no need to open the switch 13-152 for FN1_sw, FN5_sw, FN6_sw for loop elimination, and the same is true for the switch 18-135 for FN7_sw–FN9_sw. This will ensure the possibility of mains supply. Additionally, an operator can open the switch 151-300 to save the load 51. The computed FN-based resiliency metrics are shown in Fig. 10. The DSO should choose the configuration with the highest score, i.e. FN3_sw. To make the transition to this configuration the operator should close the switches 13-152 and 54-94 and open the switches 151-300 and 55-81.

Contingency III: It is assumed that a severe hurricane hit the system, and about the half of the nodes and connecting lines are damaged (Fig. 11). As a result of the hurricane, two islands are formed. The supply of critical loads is only possible with FN3_sw and FN4_sw. After the significant changes in architecture, both FN3_sw and FN4_sw demonstrate about the same resiliency rate. However, FN4_sw should be preferable, since it connects the CL, node 76, and the DER, node 56, with the shortest path.

6. Conclusions

In this study, a method to determine long-term strategies for power distribution system (PDS) resiliency enhancement is presented. The proposed methodology is quantitative, comparable for different systems, and can be utilized by power system planning engineers to select among multiple system upgrade options enabling resiliency. Particularly, the topology-based and feasible-network (FN)-based metrics were applied for the resiliency-driven distribution system planning. Two composite resiliency indices, TRI and FNRI, are introduced to provide distribution planning engineers with an insight about the resiliency of a network and to choose an appropriate decision about the infrastructural investments. The pros and cons of the both resiliency-targeted algorithms are discussed. The TRI is calculated from the topology-based resiliency, which is derived from the graph theory. This approach can be sufficient for PDS planning strategies aimed on the additional switches installation, but is not suggested for strategies focused on DERs deployment. The proposed FN-based approach is directly targeted on CLs saving and takes into account the number and locations of available sources. The FNRI can also be employed in the planning phase to justify the cost of associated infrastructure improvements.

The effectiveness of both TRI and FNRI were substantiated on the modified IEEE 123 node system and the results show the resiliency improvements numerically. For the considered PDS, the planning

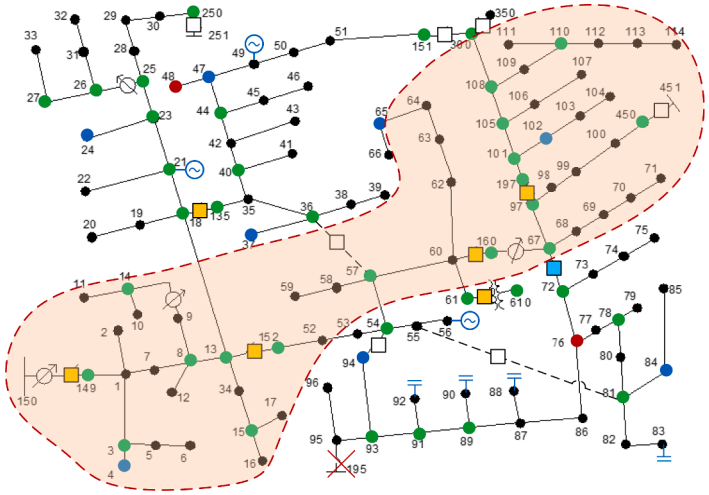

Fig. 11. Contingency III scenario: a hurricane hit the system

strategies focused on adding tie-lines with automated switches demonstrated TRI improvement ratio of 1.5578, and the FNRI improvement ratio of 1.4955. The TRI and the FNRI scores are coordinate with a 4% tolerance, which demonstrates a good consistency of both composite resiliency indices with each other. The best resiliency improvement was supervised when DERs and tie-line switches were injected simultaneously, and the highest FNRI improvement ratio reached 3.5172.

The use of AHP is computationally efficient and fast, and the inconsistency of the solution does not exceed 5.1% for the studied cases. The employed pairwise comparison can be modified as necessary, depending on how the system planning engineer defines resiliency factors. This allows flexibility in the method to incorporate more factors into calculations. Applicability of the FN-based method for post-contingency operational decision-making was examined with three contingency scenarios, including faults within the feeder and severe damages caused by weather unfavorable events. After planning and implementation are done, the PDS can be tuned to its most resilient state. When a contingency happens, the proposed metrics can be utilized for providing a DSO with the real-time information about the most resilient network configuration for critical loads restoration. With respect to the system's operating state, the distribution system operator can choose the most appropriate FN, considering the results of cost-benefit analysis for connecting additional DERs at the certain point of time. This allows to ensure that all CLs are energized even in post-contingency mode, and that a system operates in the most resilient configuration. Planning strategies should consider each state and utility's unique circumstances, as well as recognize that the potential value to the PDS of any particular distributed energy source and/or automated switch deployment is dependent on location and performance, among other factors.

Extension of the proposed method to account for varying operational conditions (i.e. for varying load demand) will be considered in a future work. The resiliency-driven strategies presented in this paper are mostly focused on the PDS planning and anticipation of impending threats and can serve as an auxiliary tool for post-contingence planning. During prospective research the aspects of network's reconfiguration after the contingency will be studied in more detail, and operational (post-contingency) decisions the network operator can make to reduce the consequences will be determined. Such a study may include (a) development of a separate set of resiliency metrics for restoration stage, (b) utilization of graph-search algorithms to find an optimal reconfiguration problem solution, (c) evaluation of how quickly the PDS can recover with minimum cost and restore supply to downed CLs. As a result, the system should be able to effectively withstand the threat by minimizing damage to its components and provide continuous service to the CLs.

Credit author statement

The evaluation of the authors' contribution:

Illia Diahovchenko: creation of the research concept, developing of the mathematical model, research model development and simulation, analysis of the obtained results, manuscript preparation.

Gowtham Kandaperumal: research model development and simulation, analysis of the obtained results.

Anurag K. Srivastava: heading of the research, creation of the research concept, advising, reviewing and editing.

Zoia I. Maslova: developing of the mathematical model.

Serhii M. Lebedka: analysis of the obtained results, reviewing.

Declaration of Competing Interest

1) This material has not been published in whole or in part elsewhere; 2) the manuscript is not currently being considered for publication in another journal; 3) authors do not have conflict of interest regarding the authorship and the content of the manuscript; 4) all authors have been personally and actively involved in substantive work leading to the manuscript, and will hold themselves jointly and individually responsible for its content.

Appendix

Fig. A1.
Table AI.
Table AII.
Table AIII.

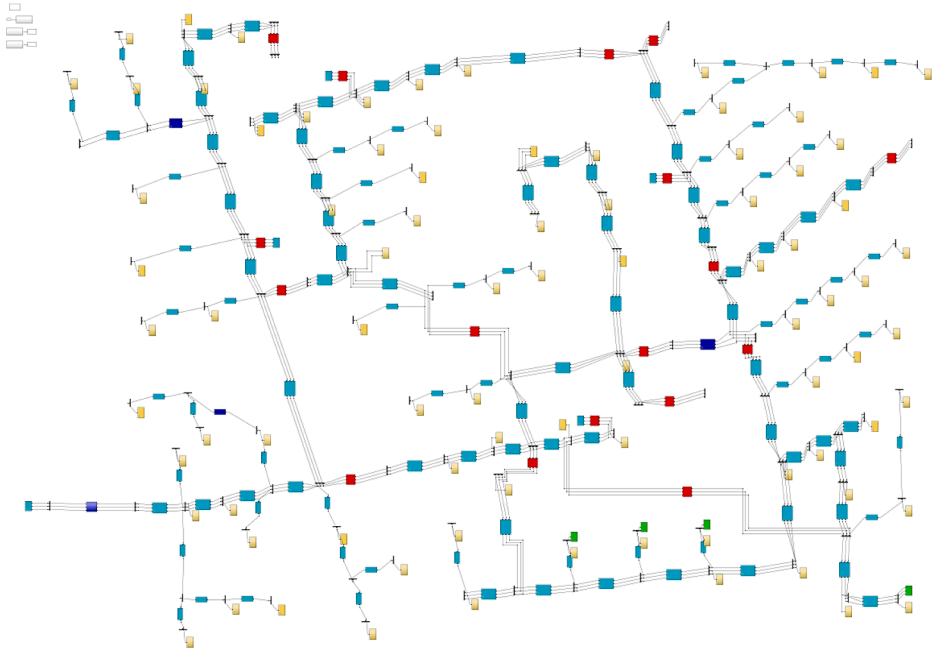

Fig. A1. Modified IEEE 123 bus system in MATLAB Simulink

Table AI
The reference designation for the studied power distribution system in MATLAB simulink.

Element	Description	Element	Description
	Main source (swing bus 150)		Load (three-phase)
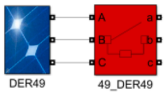	Three-phase DG with the NO connecting switch		Three-phase switch (switch is NC)
	Three-phase voltage regulator		Shunt capacitor (three-phase)
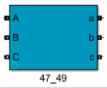	Three-phase line		Bus (three-phase)

Table AII
Possible networks and their combination to feasible networks for cases 1-3 (the PDS is reinforced by means of additional DG installation).

FN	Possible networks
FN1	PN1, PN4, PN7, PN9, PN11, PN13, PN16, PN18, PN20, PN22, PN23, PN27, PN30, PN32, PN34, PN36, PN38, PN40, PN42, PN44, PN46
FN2	PN2, PN5, PN8, PN10, PN12, PN14, PN17, PN19, PN21, PN23, PN25, PN28, PN31
FN3	PN3, PN15, PN26
FN4	PN6, PN29
FN5	PN33, PN35, PN37, PN39
FN6	PN41, PN43, PN45, PN47

Table AIII
Possible networks and their combination to feasible networks for cases 4-7 (the PDS is reinforced by means of additional DG and switches combining).

FN	Possible networks	SO
FN1_sw	PN1, PN10, PN29, PN38, PN44, PN55, PN64, PN70, PN79, PN85, PN116, PN128, PN134, PN137, PN140 (15 pieces)	2
FN2_sw	PN2, PN14, PN19, PN30, PN35, PN48, PN52, PN56, PN65, PN76, PN80, PN89, PN94, PN107, PN113, PN119, PN122, PN146, PN149, PN152, PN155 (21 pieces)	0
FN3_sw	PN3, PN15, PN20, PN31, PN36, PN49, PN53, PN57, PN66, PN77, PN81, PN90, PN95, PN108, PN114, PN120, PN123, PN147, PN150, PN153, PN156 (21 pieces)	2
FN4_sw	PN4, PN16, PN21, PN32, PN37, PN50, PN54, PN59, PN68, PN78, PN82, PN91, PN96, PN109, PN115, PN121, PN124, PN148, PN151, PN154, PN157 (21 pieces)	2
FN5_sw	PN5, PN12, PN33, PN42, PN46, PN58, PN67, PN73, PN83, PN87, PN117, PN132, PN135, PN138, PN143 (15 pieces)	4
FN6_sw	PN6, PN13, PN34, PN43, PN47, PN60, PN69, PN75, PN84, PN88, PN118, PN133, PN136, PN139, PN145 (15 pieces)	4
FN7_sw	PN7, PN22, PN26, PN39, PN61, PN71, PN97, PN100, PN104, PN110, PN125, PN129, PN141 (13 pieces)	2
FN8_sw	PN8, PN24, PN27, PN40, PN62, PN72, PN98, PN102, PN105, PN111, PN126, PN130, PN142 (13 pieces)	4
FN9_sw	PN9, PN25, PN28, PN41, PN63, PN74, PN99, PN103, PN106, PN112, PN127, PN131, PN144 (13 pieces)	4
FN10_sw	PN11, PN51, PN86 (3 pieces)	2
FN11_sw	PN17, PN 92 (2 pieces)	4
FN12_sw	PN18, PN 93 (2 pieces)	4
FN13_sw	PN23, PN45, PN 101 (3 pieces)	4

References

[1] "Distribution System Planning: Proactively Planning for More Distributed Assets at the Grid Edge," 2018.
[2] A. Silverstein, "A customer-focused framework for electric system resilience," no. May, 2018.
[3] A. Gholami, F. Aminifar, and M. Shahidehpour, "Front lines against the darkness: enhancing the resilience of the electricity grid through microgrid facilities," IEEE Electrif. Mag., 2016.
[4] A. B. Smith, "2020 U.S. billion-dollar weather and climate disasters in historical context," 2021.
[5] NOAA National Centers for Environmental Information (NCEI), "U.S. Billion-Dollar Weather and Climate Disasters," 2020. [Online]. Available: https://www.ncdc.noaa.gov/billions/.
[6] G. Liang, S. R. Weller, J. Zhao, F. Luo, and Z. Y. Dong, "The 2015 Ukraine Blackout: Implications for False Data Injection Attacks," IEEE Trans. Power Syst., 2017.
[7] Executive Office of the President of the United States, "Economic Benefits of Increasing Electric Grid Resilience To Weather Outages," 2013.
[8] A. Arab, A. Khodaei, Z. Han, S.K. Khator, Proactive Recovery of Electric Power Assets for Resiliency Enhancement, IEEE Access, 2015.
[9] D. K. Mishra, M. J. Ghadi, A. Azizivahed, L. Li, and J. Zhang, "A review on resilience studies in active distribution systems," Renewable and Sustainable Energy Reviews. 2021.

[10] G. Kandaperumal, A.K. Srivastava, Resilience of the electric distribution systems: Concepts, classification, assessment, challenges, and research needs, IET Smart Grid, 2020.
[11] R. E. Fisher and M. Norman, "Developing measurement indices to enhance protection and resilience of critical infrastructure and key resources," J. Bus. Contin. Emer. Plan., 2010.
[12] A. Kwasinski, "Quantitative model and metrics of electrical grids' resilience evaluated at a power distribution level," Energies, 2016.
[13] P. Bajpai, S. Chanda, and A. K. Srivastava, "A Novel Metric to Quantify and Enable Resilient Distribution System Using Graph Theory and Choquet Integral," IEEE Trans. Smart Grid, 2018.
[14] A.P.J.C. Crittenden;, Index of Network resilience (INR) for urban water distribution Systems. Conference: 2012 Critical Infrastructure Symposium, At Arlington, VA, 2014.
[15] D. Henry and J. Emmanuel Ramirez-Marquez, "Generic metrics and quantitative approaches for system resilience as a function of time," Reliab. Eng. Syst. Saf., 2012.
[16] D. A. Reed, K. C. Kapur, and R. D. Christie, "Methodology for assessing the resilience of networked infrastructure," IEEE Syst. J., 2009.
[17] A. Shahbazi, J. Aghaei, S. Pirouzi, T. Niknam, M. Shafie-khah, and J. P. S. Catalão, "Effects of resilience-oriented design on distribution networks operation planning," Electr. Power Syst. Res., 2021.
[18] S. Chanda and A. K. Srivastava, "Defining and Enabling Resiliency of Electric Distribution Systems with Multiple Microgrids," IEEE Trans. Smart Grid, 2016.
[19] Tushar, V. Venkataramanan, A. Srivastava, and A. Hahn, "CP-TRAM: Cyber-Physical Transmission Resiliency Assessment Metric," IEEE Trans. Smart Grid, 2020.
[20] J. Xu, T. Zhang, Y. Du, W. Zhang, T. Yang, and J. Qiu, "Islanding and dynamic reconfiguration for resilience enhancement of active distribution systems," Electr. Power Syst. Res., 2020.
[21] Whitehouse.gov, Presidential Policy Directive - Critical Infrastructure Security and Resilience, PPD-21, The White House, 2003.
[22] L. Mehigan, J. P. Deane, B. P. Ó. Gallachóir, and V. Bertsch, "A review of the role of distributed generation (DG) in future electricity systems," Energy. 2018.
[23] S.Y. Shevchenko, V.V. Volokhin, I.M. Diahovchenko, Power quality issues in smart grids with photovoltaic power stations, Energetika 63 (4) (2017).
[24] R. C. Lotero and J. Contreras, "Distribution system planning with reliability," IEEE Trans. Power Deliv., 2011.
[25] I. Diahovchenko, M. Kolcun, Z. Čonka, V. Savkiv, R. Mykhailyshyn, Progress and Challenges in Smart Grids: Distributed Generation, Smart Metering, Energy Storage and Smart Loads," Iran, J. Sci. Technol. Trans. Electr. Eng. (2020).
[26] A. Uniyal and S. Sarangi, "Optimal network reconfiguration and DG allocation using adaptive modified whale optimization algorithm considering probabilistic load flow," Electr. Power Syst. Res., 2020.
[27] I. Diahovchenko and Z. Viacheslav, "Optimal composition of alternative energy sources to minimize power losses and maximize profits in distribution power network," in 2020 IEEE 7th International Conference on Energy Smart Systems, ESS 2020 - Proceedings, 2020.
[28] K. Mahmoud, N. Yorino, and A. Ahmed, "Optimal Distributed Generation Allocation in Distribution Systems for Loss Minimization," IEEE Trans. Power Syst., 2016.
[29] K. Zou, A. P. Agalgaonkar, K. M. Muttaqi, and S. Perera, "Distribution system planning with incorporating DG reactive capability and system uncertainties," IEEE Trans. Sustain. Energy, 2012.
[30] E. Naderi, H. Seifi, and M. S. Sepasian, "A dynamic approach for distribution system planning considering distributed generation," IEEE Trans. Power Deliv., 2012.
[31] S. A. Arefifar, Y. A. R. I. Mohamed, and T. H. M. El-Fouly, "Optimum microgrid design for enhancing reliability and supply-security," IEEE Trans. Smart Grid, 2013.
[32] A. Heidari, V. G. Agelidis, and M. Kia, "Considerations of sectionalizing switches in distribution networks with distributed generation," IEEE Trans. Power Deliv., 2015.
[33] G. Celli and F. Pilo, "Optimal sectionalizing switches allocation in distribution networks," IEEE Trans. Power Deliv., 1999.
[34] J. C. López, J. F. Franco, and M. J. Rider, "Optimisation-based switch allocation to improve energy losses and service restoration in radial electrical distribution systems," IET Gener. Transm. Distrib., 2016.
[35] L. S. De Assis, J. F. V. González, F. L. Usberti, C. Lyra, C. Cavellucci, and F. J. Von Zuben, "Switch allocation problems in power distribution systems," IEEE Trans. Power Syst., 2015.
[36] Y. Xu, C. C. Liu, K. P. Schneider, and D. T. Ton, "Placement of Remote-Controlled Switches to Enhance Distribution System Restoration Capability," IEEE Trans. Power Syst., 2016.
[37] I. Diahovchenko, G. Kandaperumal, A.K. Srivastava, Distribution Power System Resiliency Improvement Using Distributed Generation and Automated Switching. 2019 IEEE 6th International Conference on Energy Smart Systems, IEEE ESS, 2019.
[38] J. L. Latchman, "V. Pisarenko and M. Rodkin: Heavy-Tailed Distributions in Disaster Analysis," Math. Geosci., 2011.
[39] T. L. Saaty, "Decision making with the analytic hierarchy process," Int. J. Serv. Sci., 2008.
[40] J.M. Hernandez, P. Van Mieghem, Classification of graph metrics, Delft Univ. Technol. Mekelweg, Netherlands, 2011.
[41] H. Kim and R. Anderson, "Temporal node centrality in complex networks," Phys. Rev. E - Stat. Nonlinear, Soft Matter Phys., 2012.
[42] A. Yazdani, R. A. Otoo, and P. Jeffrey, "Resilience enhancing expansion strategies for water distribution systems: A network theory approach," Environ. Model. Softw., 2011.
[43] F. Radicchi, "Predicting percolation thresholds in networks," Phys. Rev. E - Stat. Nonlinear, Soft Matter Phys., 2015.
[44] M. Molloy and B. Reed, "A critical point for random graphs with a given degree sequence," Random Struct. Algorithms, 1995.
[45] T. Kalisky, R. Cohen, D. ben-Avraham, and S. Havlin, "Tomography and Stability of Complex Networks," 2012.
[46] F. Meng, G. Fu, R. Farmani, C. Sweetapple, and D. Butler, "Topological attributes of network resilience: A study in water distribution systems," Water Res., 2018.
[47] A. Ganesh, L. Massoulié, and D. Towsley, "The effect of network topology on the spread of epidemics," in Proceedings - IEEE INFOCOM, 2005.
[48] P. Van Mieghem, J. Omic, and R. Kooij, "Virus spread in networks," IEEE/ACM Trans. Netw., 2009.
[49] M.J.F. Alenazi, J.P.G. Sterbenz, Comprehensive comparison and accuracy of graph metrics in predicting network resilience. 2015 11th International Conference on the Design of Reliable Communication Networks, DRCN, 2015, p. 2015.
[50] V. Volokhin, I. Diahovchenko, V. Kurochkina, M. Kanálik, The influence of nonsinusoidal supply voltage on the amount of power consumption and electricity meter readings, Energetika 63 (1) (2017).
[51] W. H. Kersting, "Radial distribution test feeders," Proc. IEEE Power Eng. Soc. Transm. Distrib. Conf., 2001.
[52] E. Cotilla-Sanchez, P. D. H. Hines, C. Barrows, and S. Blumsack, "Comparing the topological and electrical structure of the North American electric power infrastructure," IEEE Syst. J., 2012.
[53] A.L. Barabási, R. Albert, Emergence of scaling in random networks, Science 80-. (1999).